

## RESEARCH

# MEBS, a software platform to evaluate large (meta)genomic collections according to their metabolic machinery: unraveling the sulfur cycle

Valerie De Anda<sup>1,\*</sup>, Icoquih Zapata-Peñasco<sup>2</sup>,  
Augusto Cesar Poot-Hernandez<sup>3</sup>, Luis E. Eguiarte<sup>1</sup>,  
Bruno Contreras-Moreira<sup>4,5,\*</sup> and Valeria Souza<sup>1,\*</sup>

<sup>1</sup>Departamento de Ecología Evolutiva, Instituto de Ecología, Universidad Nacional Autónoma de México, 70-275, Coyoacán 04510, D.F., México, <sup>2</sup>Dirección de Investigación en Transformación de Hidrocarburos, Instituto Mexicano del Petróleo, Eje Central Lázaro Cárdenas, Norte 152, Col. San Bartolo Atepehuacan, 07730, México, <sup>3</sup>Departamento de Ingeniería de Sistemas Computacionales y Automatización. Sección de Ingeniería de Sistemas Computacionales. Instituto de Investigaciones en Matemáticas Aplicadas y en Sistemas. Circuito Escolar 3000, Cd. Universitaria, 04510 Ciudad de México, <sup>4</sup>Estación Experimental de Aula Dei, Consejo Superior de Investigaciones Científicas (EEAD-CSIC), Avda. Montañana, 1005, Zaragoza 50059, Spain and <sup>5</sup>Fundación ARAID, calle María de Luna 11, 50018 Zaragoza, Spain

\*Corresponding address. Valerie de Anda, Instituto de Ecología, Universidad Nacional Autónoma de México, 70-275, Coyoacán 04510, D.F., México; Tel: (+52)5556229006; Fax: +52-5556228995; E-mail [valdeanda@ciencias.unam.mx](mailto:valdeanda@ciencias.unam.mx); Bruno Contreras Moreira, Estación Experimental de Aula Dei, Avda. Montañana, 1005, Zaragoza 50059; Spain; Tel: (+34)976716089; Fax: +34 976716145; E-mail [bcontreras@eead.csic.es](mailto:bcontreras@eead.csic.es); Valeria Souza, Instituto de Ecología, Universidad Nacional Autónoma de México, 70-275, Coyoacán 04510, D.F., México; Tel: (+52)5556229006; Fax: +52-5556228995; E-mail [souza@unam.mx](mailto:souza@unam.mx)

## Abstract

The increasing number of metagenomic and genomic sequences has dramatically improved our understanding of microbial diversity, yet our ability to infer metabolic capabilities in such datasets remains challenging. We describe the Multigenomic Entropy Based Score pipeline (MEBS), a software platform designed to evaluate, compare, and infer complex metabolic pathways in large “omic” datasets, including entire biogeochemical cycles. MEBS is open source and available through [https://github.com/eead-csic-compbio/metagenome\\_Pfam\\_score](https://github.com/eead-csic-compbio/metagenome_Pfam_score). To demonstrate its use, we modeled the sulfur cycle by exhaustively curating the molecular and ecological elements involved (compounds, genes, metabolic pathways, and microbial taxa). This information was reduced to a collection of 112 characteristic Pfam protein domains and a list of complete-sequenced sulfur genomes. Using the mathematical framework of relative entropy ( $H'$ ), we quantitatively measured the enrichment of these domains among sulfur genomes. The entropy of each domain was used both to build up a final score that indicates whether a (meta)genomic sample contains the metabolic machinery of interest and to propose marker domains in metagenomic sequences such as DsrC (PF04358). MEBS was benchmarked with a dataset of 2107 non-redundant microbial genomes from RefSeq and 935 metagenomes from MG-RAST. Its performance, reproducibility,

Received: 13 June 2017; Revised: 9 September 2017; Accepted: 1 October 2017

© The Author 2017. Published by Oxford University Press. This is an Open Access article distributed under the terms of the Creative Commons Attribution License (<http://creativecommons.org/licenses/by/4.0/>), which permits unrestricted reuse, distribution, and reproduction in any medium, provided the original work is properly cited.

and robustness were evaluated using several approaches, including random sampling, linear regression models, receiver operator characteristic plots, and the area under the curve metric (AUC). Our results support the broad applicability of this algorithm to accurately classify (AUC = 0.985) hard-to-culture genomes (e.g., *Candidatus Desulfurudis audaxviator*), previously characterized ones, and metagenomic environments such as hydrothermal vents, or deep-sea sediment. Our benchmark indicates that an entropy-based score can capture the metabolic machinery of interest and can be used to efficiently classify large genomic and metagenomic datasets, including uncultivated/unexplored taxa.

**Keywords:** metabolic machinery; metagenomics; omic-datasets; Pfam domains; relative entropy; sulfur cycle; multigenomic entropy-based score

## Background

Over the last 15 years, the enormous advances in high-throughput sequencing technologies have revolutionized the field of microbial ecology, dramatically improving our understanding of life's microbial diversity to an unprecedented level of detail [1–4].

Nowadays, accessing the total repertoire of genomes within complex communities by means of metagenomics is becoming a standard and routine procedure in order to attain the full insight of the diversity, ecology, evolution, and functional makeup of the microbial world [5]. Furthermore, the accurate reconstruction of microbial genomes and draft-populations from environmental metagenomic studies has been shown to be a powerful approach [6–10], providing clues about the potential metabolic strategies of hard-to-culture microbial lineages by linking the functional mechanisms that support specific metabolisms with taxonomic, systematic, and ecological contexts of that lineage [8].

Despite the accelerated accumulation of large collections of metagenomic and genomic sequences, our ability to analyze, evaluate, and compare complex metabolic capabilities in large-scale “omic” datasets remains biologically and computationally challenging [11]. Predicting the metabolic potential is a key step in describing the relationship between a microbial community and its ecosystem function. This is largely performed by mapping the protein coding genes of “omic” data onto reference pathway databases such as MetaCyc [12] or KEGG [13] based on their homology to previously characterized genes [14]. The currently available methods for metabolic pathway prediction or reconstruction rely on the use of several metrics to infer the overall repertoire of metabolic pathways present in a given metagenomic dataset (e.g., MinPath [14], HUMAnN [15], PRMT [16], MetaPathways [17]).

However, due to the challenges involved in testing meaningful biological hypotheses with complex data, only a small proportion of the metabolic information derived from these datasets is eventually used to draw ecologically relevant conclusions. In this regard, most of the microbial ecology-derived “omic” studies have been mainly focused on either: (i) developing a broad description of the metabolic pathways within a certain environment [18, 19]; (ii) analyzing the relative abundance of marker genes involved in several metabolic processes and in certain ecosystems (e.g., primary productivity, decomposition, biogeochemical cycling) [20–24]; or (iii) discovering differentially abundant, shared or unique functional units (genes, proteins, or metabolic pathways) across several environmental metagenomic samples [25–27].

Therefore, in order to integrate all available omics data, we propose a novel approach to reduce the complexity of targeted metabolic pathways involved in several integral ecosystem processes—such as entire biogeochemical cycles—into a single informative score, called the Multigenomic Entropy-Based Score (MEBS). This approach is based on the mathematical ra-

tionalization of Kullback-Leibler divergence, also known as relative entropy  $H'$  [28]. Relative entropy has been widely applied in physics, communication theory, and statistical inference, and it is interpreted as a measure of disorder, information, and uncertainty, respectively [29]. Here we use the communication theory concept of  $H'$  to summarize the information derived from the metabolic machinery encoded by the protein coding genes of “omic” datasets. The application of this metric in biology was originally developed by Stormo and colleagues, who identified binding sites that regulate gene transcription [30].

In order to evaluate the performance of our approach, we selected the sulfur cycle (from now on, S-cycle) because this is one of the most metabolically and ecologically complex biogeochemical cycles, but there are few studies analyzing the complete repertoire (genes, proteins, or metabolic pathways) involved in the mobilization of inorganic-organic sulfur compounds through microbial-catalyzed reactions at a planetary scale [20, 31–35].

## MEBS Description

MEBS (MEBS, RRID:SCR\_015708) runs in Linux systems [36]. For practical purposes, the MEBS algorithm was divided into 4 stages, summarized in Fig. 1 and explained below.

### Stage 1: manual curation of Sulfur cycle and “omic” datasets

#### Sulfur taxonomic representatives

A dataset comprehensively covering the currently known representatives of the S-cycle was obtained from primary literature and the MetaCyc database [12]. Each taxonomic representative (at the genus or species level) was selected under the criteria of having evidence suggesting their physiological and biochemical involvement in the degradation, reduction, oxidation, or disproportionation of sulfur compounds. Then, each taxonomic representative was scanned against our genomic dataset (see further details below) in order to obtain a list containing the completely sequenced and non-redundant genomes of the S-cycle. The resulting Sulfur list (or “Suli”) currently contains 161 curated genomes and was used as the first input of the pipeline. Both the manually curated taxonomic representatives and Suli can be found in Table S1.

#### Random taxonomic representatives (Rlist)

As a negative control, we generated 1000 lists of genomes that are not particularly enriched on sulfur metabolic preferences. Each list contains 161 random genomes, the same number of microorganisms included in Suli. These lists were obtained by randomly subtracting from the genomic dataset (see below) 161 Refseq accession numbers and their corresponding names.

# MEBS MULTIGENOMIC ENTROPY BASED SCORE

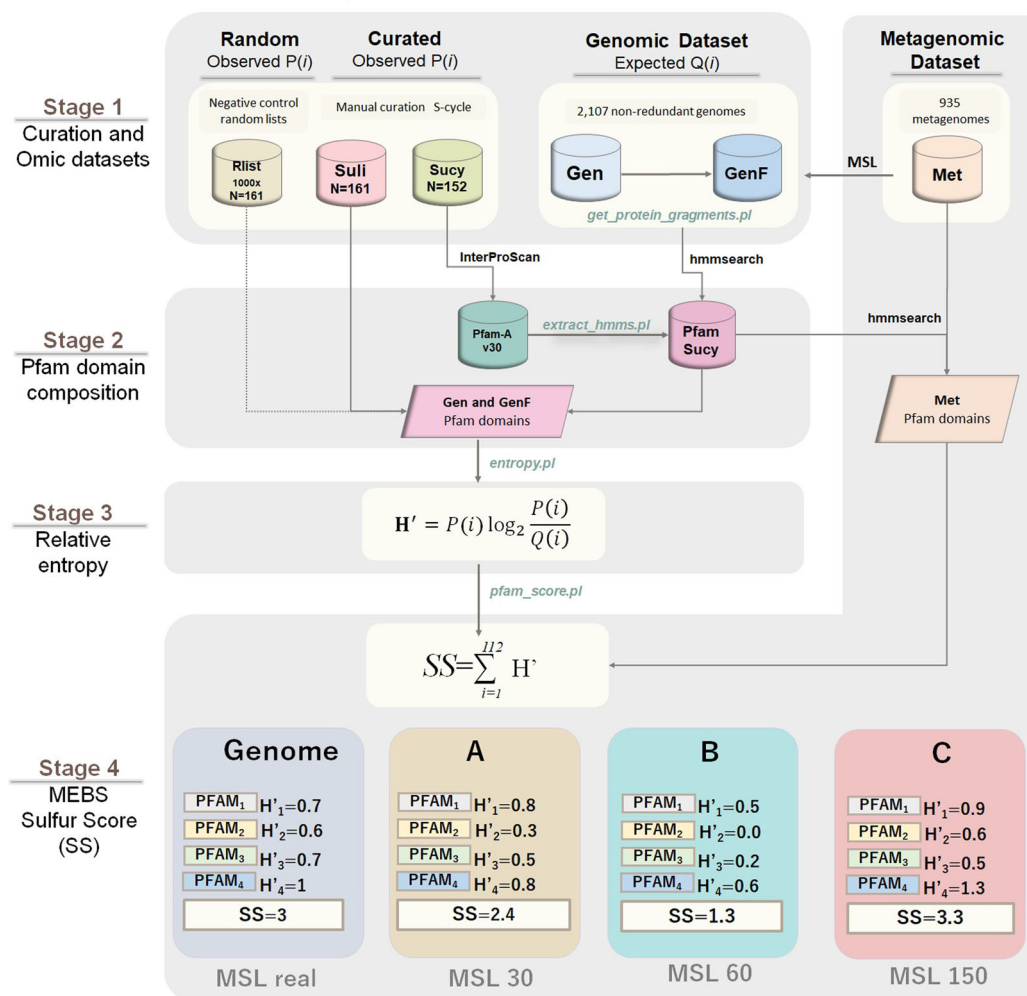


**Figure 1:** Schematic representation of the 4 stages of the MEBS algorithm focusing on the S-cycle. The first step consists of the systematic curation of a database containing the metabolic information of the S-cycle, which is reduced to a FASTA file of proteins involved (Sucy) and a list of 161 related microorganisms (Suli). A thousand lists of 161 random-sampled genomes were used as negative control (Rlist). The training dataset comprises 2107 genomes (Gen), which were fragmented in different sizes by considering the mean size length (MSL) of 935 metagenomes (Met). In the second stage, the domain composition of Sucy proteins is obtained by scanning Pfam-A, resulting in the Pfam-Sucy database. Then, the relative entropy ( $H'$ ) of each Sucy-Pfam domain is obtained in the third stage. Finally, the precomputed entropies in Gen and GenF are used to evaluate full-length genomic sequences (real) and metagenomic sequences of variable MSL (in this example A, B, and C).

### Metabolic pathways and genes

We gathered and classified the metabolic pathways involved in the S-cycle from the primary literature and 2 experimentally validated curated databases: KEGG (KEGG, [RRID:SCR.012773](https://pubmed.ncbi.nlm.nih.gov/112773/)) [13] and MetaCyc (MetaCyc, [RRID:SCR.007778](https://pubmed.ncbi.nlm.nih.gov/100778/)) [12]. All the molecular information was then combined into a single database named Sucy (for **s**ulfur **c**ycle). Sucy currently contains 152 genes and 48 enzyme classification numbers annotated in the Enzyme classification [37] (Table S2). The 152 FASTA sequences of the proteins encoded by these genes were downloaded from UniProt [38] and used as the second input of the pipeline.

### Genomic dataset (Gen)

At the time of the analysis (December 21, 2016), a total of 4158 genomes were available from RefSeq database [39]. For comparative genomic purposes, we removed redundancy in this

large dataset by using the Web interface [40, 41]. As a phylogenomic distance measure, we used a modified version of the Genomic Similarity Score (GSSb) [41]; we selected the most tolerant threshold of 0.95 (so as not to drop many sequenced genomes) and default parameters, resulting in 2107 clusters containing similar genomes, ordered by size (largest to smallest). Then, the largest genome representative for each group was searched in the NCBI genome assembly summary file [42] and downloaded from the NCBI FTP site [43].

### Metagenomic dataset (Met)

We used the Meta Genome Rapid Annotation using Sub-system Technology server (MG-RAST, [RRID:SCR.004814](https://pubmed.ncbi.nlm.nih.gov/144814/)) [44] to download metagenomes that: (i) were publicly available; (ii) contained associated metadata; and (iii) had been isolated from well-defined environments (i.e., rivers, soil, biofilms),

discarding host-associated microbiome sequences (i.e., human, cow, chicken). In addition, we included 35 unpublished metagenomes derived from sediment, water, and microbial mats from Cuatro Ciénegas, Coahuila (CCC), Mexico. The latter were also submitted and annotated in the MG-RAST server and will be described in depth elsewhere. The resulting collection of 935 FASTA files ( $\approx 500$  GB), containing gene-called protein sequences (MG-RAST stage 350), were downloaded from the RESTful MG-RAST API [45]. While these metagenomes were evaluated and scored in STAGE 4, they were also analyzed to estimate their mean sequence length, considering that the fragmented nature of metagenomic sequences would have an impact on homology detection, depending on the length of the reads [46, 47]. Therefore, we measured the mean size length (MSL) of the peptide sequences of the 935 metagenomes in Met and the 152 curated proteins in Suci, which are summarized in Fig. S1. It was observed that the MSL of Met varies broadly, with a majority of metagenomic peptides with  $MSL \leq 30$  aa, and that Suci proteins range from 49 to 1020 aa, with  $MSL = 349$  aa. According to this distribution, the metagenomes in Met were grouped into 7 well-defined categories:  $MSL \leq 30$ ,  $\leq 60$ ,  $\leq 100$ ,  $\leq 150$ ,  $\leq 200$ ,  $\leq 250$ ,  $\leq 300$  aa.

#### Fragmented genomic dataset (GenF)

In order to simulate the observed variability of MSL across metagenomes, protein sequences encoded in the genomic dataset (Gen, containing 2107 genomes) were *in silico* sheared with Perl script *get.protein.fragments.pl* into the 7 MSL categories defined above (30 to 300). This produced the GenF dataset, which currently requires up to 104 GB of disk space.

### Stage 2: domain composition of the input proteins

The annotation of protein domains in Suci was conducted using Interproscan 5.21–60.0 [48] against databases Pfam-A v30 (Pfam, [RRID:SCR.004726](#)) [49], TIGRFAM v13 (JCVI TIGRFAMS, [RRID:SCR.005493](#)) [50], and Superfamily v1.75 (SUPERFAMILY, [RRID:SCR.007952](#)) [51]. Then, the Hidden Markov Models (HMMs) from matched Pfam domains ( $n = 112$ ) were extracted from Pfam-A using script *extract.hmms.pl*. These selected HMMs were subsequently scanned against the Genomic, Genomic Fragmented, and Metagenomic datasets (from now on, “omic” datasets, see subsequent stages) using HMMER 3.0, the *hmmsearch -cut.ga* option [52].

### Stage 3: relative entropy and its use in detecting informative domains

In order to detect protein domains enriched among sulfur-based microorganisms (Suli), we used a derivative of the Kullback-Leibler divergence [28]—also known as relative entropy  $H'(i)$ —to measure the difference between probabilities  $P$  and  $Q$  (see Equation (1) below). In this context,  $P(i)$  represents the frequency of protein domain  $i$  in the 161 Suli genomes (observed frequency), while  $Q(i)$  represents its frequency in the 2107 genomes in Gen (expected frequency). The script to compute the entropy (*entropy.pl*) requires the list of the genomes of interest (Suli) and the tabular output file obtained from the scanning of Gen and GenF against the Pfam-Suci database. The obtained values of  $H'$  (in bits) capture to what extent a given Pfam domain informs about the metabolism of interest. In this case, domains with  $H'$  values close to or greater than 1 correspond to the most informative Pfam domains (enriched among S-based genomes),

whereas low  $H'$  values (close to 0) indicate non-informative ones. Negative values correspond to those observed less than expected.

$$H' = P(i) \log_2 \frac{P(i)}{Q(i)} \quad (1)$$

As a negative control, the  $H'$  of the 112 Pfam domains were recalculated in both the Gen and GenF datasets, but replacing Suli with 1000 equally sized lists of random-sampled genomes (Rlist).

We evaluated the impact of the MSL in the computed entropy values using Gen and GenF. First, we focused on detecting informative Pfam domains that could be used as possible molecular marker genes in variable-length metagenomic sequences. Specifically, we looked for domains displaying stable  $H'$  values across both Gen and GenF by using the script *plot\_cluster\_comparison.py*, which implements the following methods: K-Means, Affinity propagation, Mean-shift Spectral, Ward hierarchical, Agglomerative, DBSCAN, and Birch. All of these are part of the scikit-learn Machine Learning Python module [53].

### Stage 4: final score, interpretation, properties, and benchmark

Peptide sequences from a given genome or metagenome of interest are evaluated by first scanning their Pfam domains and then producing a final score, defined as the sum of the precomputed entropies of matched S-related Pfam domains (see Equation (2)). This score (Sulfur Score [SS] in our case) summarizes the information content of the metabolic machinery of interest. In this context, informative sulfur protein domains would contribute to higher SS, whereas non-informative ones would decrease it. This is an extension of procedures originally developed for the alignment of DNA and protein motifs, in which individual positions are independent and additive and can be simply summed up to obtain the total weight or information content [30]. Instead of aligning sequences, in our context we added up the entropy values of the Pfam domains matched in a given “omic” sample (resulting from scanning the sample of interest against Pfam-Suci), from which a total weight (SS) is computed by using script *pfam\_score.pl*.

$$SS = \sum_{i=1}^{112} H' \quad (2)$$

Datasets in which the majority of informative S-cycle protein domains are represented will yield a high SS; in contrast, low SS values should be expected if proteins involved in the S-cycle are not particularly enriched.

#### MSL

As the calculation of the SS depends on the MSL of the omic sample of interest, script *pfam\_score.pl* supports option `-size` in amino acid residues (aa). In this way, appropriate precomputed  $H'$  values for Pfam domains can be selected to produce the final score. Currently 30, 60, 100, 150, 200, 250, 300, and real sizes are supported.

#### Metabolic pathway completeness and KEGG visualization

The presence-absence patterns of Pfam domains belonging to particular pathways can be exploited to compute metabolic completeness. This optional task is invoked with

parameter `-keggmap` and a TAB-separated file mapping Pfam identifiers to KEGG Orthology entries (KO numbers) and the corresponding pathway in SUCY (see Table S3). To compute completeness, the total number of domains involved in a given pathway (i.e., sulfate reduction, sulfide oxidation) must be retrieved from the SUCY database (See Table S2). Then, the protein domains currently present in any given sample are divided by the total number of domains in the pre-defined pathway. The script produces: (i) a detailed report of the metabolic pathways of interest and (ii) a list of KO numbers with Hex color codes, corresponding to KO matches in the omic sample, which can be exported to the KEGG Mapper-Search & Color Pathway tool (see Fig. S2) [54].

#### Properties and performance of SS

Since the outcome of the final score (SS) largely depends on the list of microorganisms involved in the metabolism of interest (in our case, Suli) and the Pfam domains found in the input protein sequences ( $n = 112$ ), we evaluated its robustness and reproducibility with several approaches. First, we compared our results with a benchmark performed 3 years ago in which we used Pfam-A v27 (instead of version 30), a genomic dataset containing 1528 non-redundant genomes (579 fewer genomes than our current Genomic dataset), and an input list of 156 genomes of interest (5 fewer than our current Suli). Second, SS estimates were compared with scores obtained by randomly selecting  $\approx 50\%$  of the 112 Pfam domains with both Gen and Met. This analysis was performed a thousand times with `pfam.score.pl -random`. Third, we benchmarked the predictive capacity of the SS in order to accurately classify genomes of S-related organisms (Suli,  $n = 161$ , positive instances), in contrast with a larger set of non-redundant genomes (Gen-Suli,  $n = 1.946$ , negative instances). Therefore, we computed the true positive rates (TPR), false positive rates (FPR), receiver operating characteristic (ROC) plots, and the resulting area under the curve (AUC) using the scikit-learn module [53].

## Results and Discussion

We present MEBS, a new open source software to evaluate, quantify, compare, and predict the metabolic machinery of interest in large “omic” datasets. The pipeline includes 4 stages. The first one consists of the systematic and targeted acquisition of the molecular and ecological information describing the metabolism of interest, represented by a list of curated microorganisms and a FASTA file of proteins involved in that metabolic network. In the second stage, the domain composition of the curated proteins is evaluated. Then, the domains enriched among the microorganisms of interest are identified by using the mathematical framework of the relative entropy ( $H'$ , third stage). Finally, the summation of the entropy of individual Pfam domains in a given genome or metagenomic dataset yields the final score (see Fig. 1).

To test the applicability of this approach, we evaluated the metabolic machinery of the S-cycle. Due to its multiple redox states and its consequences on microbiological and geochemical transformations, S-metabolism can be observed as a complex metabolic machinery, involving a myriad of genes, enzymes, organic substrates, and electron carriers, which largely depend on the surrounding geochemical and ecological conditions. For these reasons, the complete repertory involved in the metabolic machinery of the S-cycle has remained underexplored despite the massive data produced in “omic” experiments. Here, we performed an integral curation effort to describe all the elements

involved in the S-cycle and then used, as explained in the following sections, to score genomic and metagenomic datasets in terms of their sulfur relevance.

### Manual curation: the complex metabolic machinery of the sulfur cycle

In order to integrate the complete biogeochemical S-cycle, we manually curated and modeled the major processes involved in the mobilization and use of S-compounds through Earth's biosphere. This effort resulted in 2 comprehensive databases. The first one includes most of the known microorganisms (with and without complete genomes) described in the literature to be closely involved in the S-cycle (Table S1). In this database, we included representative taxa from the following metabolic sulfur guilds: (i) chemolithotrophic, colorless sulfur bacteria (CLSB: 24 genera); (ii) anaerobic phototrophs, purple sulfur bacteria (PSB: 25 genera), and green sulfur bacteria (GSB: 9 genera); (iii) sulfate-reducing bacteria (SRB: 40 genera); and (iv) deep-branch sulfur hyperthermophilic microorganisms, such as elemental sulfur-reducing (SRM: 19 genera) and oxidizers (SO: 4 genera). From all the microorganisms described to be involved in the S-cycle, at the time of the analysis, a total of 161 were found to be completely sequenced and non-redundant genomes, and these were used as the first input of the pipeline (Suli).

The second database (SUCY) contains genes, proteins, and pathways with experimental evidence linking them to the S-cycle. To compile this database, we first gathered the most important S-compounds derived from biogeochemical processes and biological catalyzed reactions. Then we classified each S-compound according to its chemical and thermodynamic nature (Gibbs free energy of formation). Finally, we classified whether each compound can be used as a source of carbon, nitrogen, energy, or as an electron donor, fermentative substrate, or terminal electron acceptor in respiratory microbial processes. The schematic representation of the manually curated effort summarizing the complexity of the sulfur biogeochemical cycle in a global scale is shown in Fig. 2.

Once we selected the microorganisms, genes, and biogeochemical processes involved, we systematically divided the metabolic machinery of the S-cycle into 28 major metabolic pathways described in Table 1. In general terms, we included pathways involved in: (i) the oxidation/reduction of inorganic S-compounds, used as source of energy, electron donor or acceptor (P1-P7, P11 and P20 and P21); (ii) the degradation of organic S-compounds, such as aliphatic sulfonates, sulfur amino acids, and organosulfonates (P8-P10, P12-P19, P22, P23, P27); (iii) the methanogenesis from methylated thiols, such as dimethyl sulfide DMS (P24), methylthio-propanoate (P25), and methanethiol (P26), which are generated in nature by different biogeochemical processes [12]; and finally, (iv) the biosynthesis of sulfolipids (SQDG) (P28), because it has been observed that some bacteria living in S-rich and P-lacking environments are able to synthesize sulfolipids, instead of phospholipids, in the membrane as an adaptation to the selective pressures of these particular environments [55]. The synthetic pathway P29 is explained in further detail in the next sections (Table 1).

After the comprehensive metabolic inventory was compiled, we linked all the elements in a single network representation of the S-metabolic machinery (Fig. 3). To the best of our knowledge, this is the first molecular reconstruction of the cycle that considers all the sulfur compounds, genes, proteins, and the corresponding enzymatic steps resulting in higher-order molecular pathways. The latter representation also highlights the

## Biogeochemical Sulfur cycle at global scale

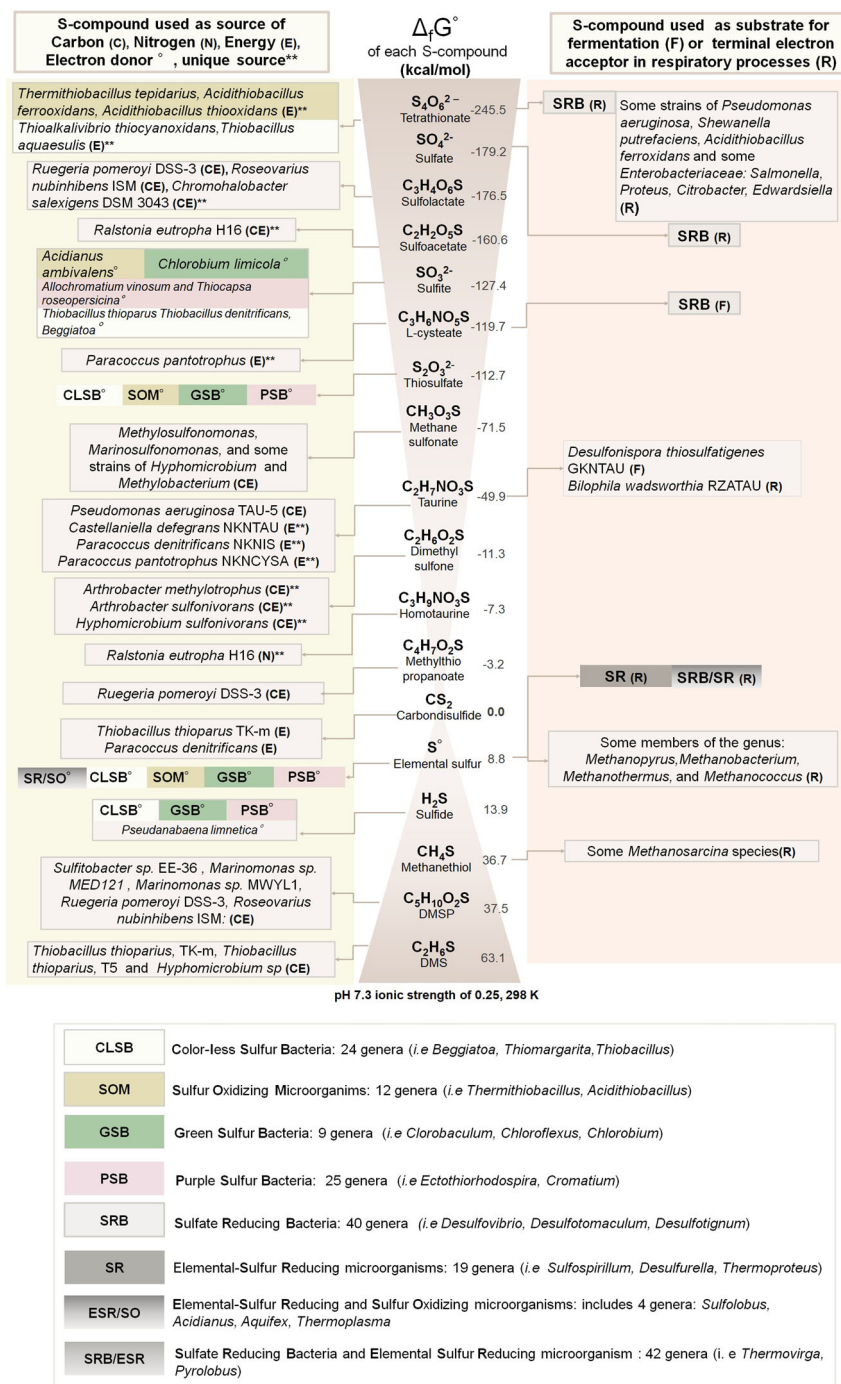


**Figure 2:** Sulfur cycle at a global scale. The most important organic and inorganic S-compounds derived from biogeochemical processes are arranged according to the Standard Gibbs free energy of formation described in Caspi et al. [12]. The left column indicates whether specific microorganisms are able to use those S-compounds as a source of carbon (C), nitrogen (N), energy (E), or electron donors (\*). Double asterisks indicate whether the S-compound is used as sole source of C, N, or E. The corresponding electron acceptors in redox-coupled reactions using the S-compound as electron donor are not shown. The right column indicates whether the S-compound is used as fermentative substrate (F) or terminal electron acceptor in respiratory processes (R). Colored boxes summarize the metabolic guilds involved in the metabolism of S-compounds in oxidation (i.e., CLSB, SOM, PSB, and GSB) or reduction (SR, SRB) processes. The complete list of S-based microorganisms (Suli) is found in Table S1. Figure based on annotations from MetaCyc [12].

**Table 1:** Metabolic pathways of global biogeochemical S-cycle

Pathway number	Metabolism <sup>a</sup>	Chemical process <sup>b</sup>	Sulfur compound	Type <sup>c</sup>	Chemical formula	Source <sup>d</sup>	Number of Pfam domains <sup>e</sup>
P1	DS	O	Sulfite	I	SO <sub>3</sub> <sup>2-</sup>	E	9
P2	DS	O	Thiosulfate	I	S <sub>2</sub> O <sub>3</sub> <sup>2-</sup>	E	10
P3	DS	O	Tetrathionate	I	S <sub>4</sub> O <sub>6</sub> <sup>2-</sup>	E	2
P4	DS	R	Tetrathionate	I	S <sub>4</sub> O <sub>6</sub> <sup>2-</sup>	E	17
P5	DS	R	Sulfate	I	SO <sub>4</sub> <sup>2-</sup>	E	20
P6	DS	R	Elemental sulfur	I	S <sup>0</sup>	E	20
P7	DS	D	Thiosulfate	I	S <sub>2</sub> O <sub>3</sub> <sup>2-</sup>	E	9
P8	DS	O	Carbon disulfide	O	CS <sub>2</sub>	E	1
P9	A	DE	Alkanesulfonate	O	CH <sub>3</sub> O <sub>3</sub> SR	S	5
P10	A	R	Sulfate	I	SO <sub>4</sub> <sup>2-</sup>	S	20
P11	DS	O	Sulfide	I	H <sub>2</sub> S	E/S	29
P12	A	DE	L-cysteate	O	C <sub>3</sub> H <sub>6</sub> NO <sub>5</sub> S	C/E	1
P13	A	DE	Dimethyl sulfone	O	C <sub>2</sub> H <sub>6</sub> O <sub>2</sub> S	C/E	3
P14	A	DE	Sulfoacetate	O	C <sub>2</sub> H <sub>2</sub> O <sub>5</sub> S	C/E	2
P15	A	DE	Sulfolactate	O	C <sub>3</sub> H <sub>4</sub> O <sub>6</sub> S	C/S	14
P16	A	DE	Dimethyl sulfide	O	C <sub>2</sub> H <sub>6</sub> S	C/S	16
P17	A	DE	Dimethylsulfoniopropionate	O	C <sub>5</sub> H <sub>10</sub> O <sub>2</sub> S	C/S/E	12
P18	A	DE	Methylthiopropionate	O	C <sub>4</sub> H <sub>7</sub> O <sub>2</sub> S	C/S	7
P19	A	DE	Sulfoacetaldehyde	O	C <sub>2</sub> H <sub>3</sub> O <sub>4</sub> S	C/S	7
P20	DS	O	Elemental sulfur	I	S <sup>0</sup>	C/S/E	7
P21	DS	D	Elemental sulfur	I	S <sup>0</sup>	C/S/E	1
P22	A	DE	Methanesulfonate	O	CH <sub>3</sub> O <sub>3</sub> S	C/S/E	7
P23	A	DE	Taurine	O	C <sub>2</sub> H <sub>7</sub> NO <sub>3</sub> S	C/S/E	11
P24	DS	M	Dimethyl sulfide	O	C <sub>2</sub> H <sub>6</sub> S	C	1
P25	DS	M	Methylthio-propionate	O	C <sub>4</sub> H <sub>7</sub> O <sub>2</sub> S	C	1
P26	DS	M	Methanethiol	O	CH <sub>4</sub> S	C	1
P27	A	DE	Homotaurine	O	C <sub>3</sub> H <sub>9</sub> NO <sub>3</sub> S	N	1
P28	A	B	Sulfolipid	O	SQDG		4
P29			Markers		Markers		12

<sup>a</sup>Metabolism: assimilative (A) inorganic compounds are reduced during biosynthesis; dissimilative (DS) inorganic compounds used as electron acceptors in energy metabolism. A large amount of electron acceptors is reduced, and the reduced product is secreted.

<sup>b</sup>Chemical process: oxidation (O); reduction (R), degradation (DE), biosynthesis (B), methanogenesis (M), disproportionation (D).

<sup>c</sup>Compound type: organic (O): sulfur atoms with covalent bonds to carbon atoms. Inorganic (I): sulfur compounds with non-carbon atoms.

<sup>d</sup>Source: sulfur compound used as source of energy (E), sulfur (S), carbon (C), nitrogen (N).

<sup>e</sup>Number of Pfam domains belonging to each metabolic pathway described in Suci (Table S2).

interconnection of pathways in terms of energy flow and the interplay of the redox gradient (organic/inorganic) of the intermediate compounds that act as key axes of organic and inorganic reactions (e.g., sulfite).

### Annotation of Pfam domains within sulfur proteins

Our approach requires the detection of structural and evolutionary units, also known as domains, in the curated list of protein sequences involved in the metabolism of interest (S-cycle in this case). The annotation of protein domains against the Pfam-A database resulted in a total of 112 domains identified in 147 proteins (out of 152). These 112 domains constitute the Pfam-Suci database and represent all the pathways listed in Table 1. Two other protein family databases were tested (TGRFAM and Superfamily), but the number of proteins with positive matches was lower than with Pfam (57 and 137, respectively), and thus the other protein family databases were not further considered.

### Preparation of omic datasets: Gen, GenF, and Met

The genomic dataset required for computing domain entropies (Gen) was obtained from public databases, as explained above in “MEBS Description.” A fragmented version of Gen, called GenF,

was generated by considering the MSL distribution of metagenomic sequences (Fig. S1).

In order to benchmark MEBS with real environmental metagenomic samples, a collection of 900 public metagenomes was obtained from MG-RAST, to which we added 35 metagenomes sampled from an ultra-oligotrophic shallow lake in México (CCC). Altogether, these 935 metagenomes set up the Met dataset.

### Using the relative entropy to recognize S-cycle domains and candidate markers

The next stage consists of the quantitative detection of informative domains (enriched among organisms in Suli) by computing their relative entropy ( $H'$ ) using Equation (1). The occurrences of each of the 112 Pfam domains in Suli and the genomic datasets were taken as observed and expected frequencies, respectively. Fig. 4A summarizes the computed  $H'$  values in real (Gen) and fragmented genomic sequences of increasing size (GenF). The results indicate that only a few Pfam domains are equally informative, regardless of the length of sequences. When  $H'$  values inferred from real, full-length proteins are compared to those of fragmented sequences, it can be seen that shorter sequences (MSL 30 and 60 aa) yield larger entropy differences than sequences of length >100 aa (see in Fig. 4B). Therefore, in order

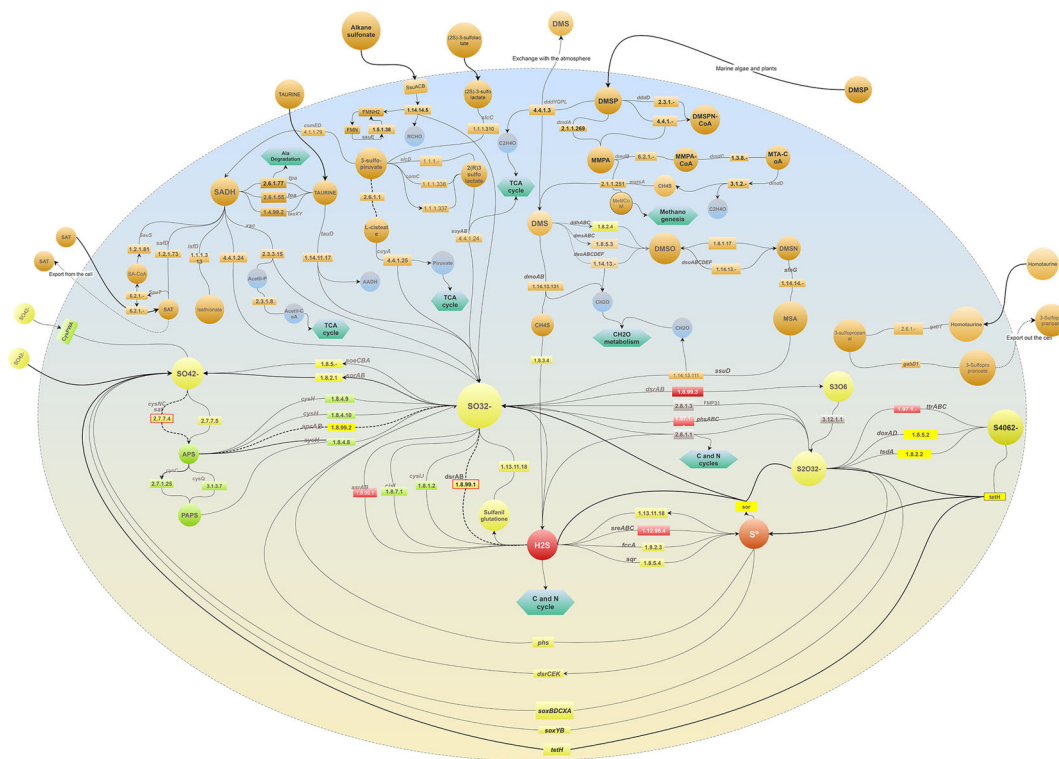


**Figure 3:** Comprehensive network representation of the machinery of the biogeochemical S-cycle in a single cell. The 28 molecular pathways involved in the metabolism of sulfur compounds described in Table 1 are included. The enzymatic steps are depicted as rectangles, followed by arrows indicating the direction of the reaction. Green hexagons represent metabolic links to other metabolisms. Bold dashed arrows indicate bidirectional reactions. Inorganic S-compounds have been arranged according to their reduction potential, from the most oxidized (yellow) to the most reduced (red) compounds. Gray rectangles indicate enzymes acting in disproportionation processes in which a reactant is both oxidized and reduced in the same chemical reaction, forming 2 separate compounds. Input biogeochemical S-compounds are shown outside and connected with bold arrows. Dashed arrows indicate S-compounds excreted out of the cell. The upper half of the modeled cell depicts the processes involved in the use of organic S-compounds (orange circles) found in natural environments and used as source of carbon, sulfur, and/or energy in several aerobic/anaerobic strains, described in Fig. 2.

to shortlist candidate marker genes, we selected those Pfam domains displaying constant, high mean  $H'$  values in Gen and GenF, low  $H'$  standard deviation (std), and a clear separation from the random distribution.

We tested several clustering methods, summarized in Fig. S3, with Ward and Birch performing best in grouping together informative protein domains with low std. However, the Ward classification was eventually selected as Birch failed to include a few Pfam domains relevant in the S-cycle (see Fig. S4). By using the Ward method, 3 well-defined clusters of Pfam domains were generated, as observed in Fig. 4C. Cluster 0 included 94 domains containing  $H'$  values ranging from  $-0.4$  to  $0.4$  and overlapping with the values obtained in the negative control explained in the next section. Cluster 1 consistently grouped together 12 Pfam domains, listed in Table 2, with high entropy and low std, and can therefore be proposed as molecular markers in metagenomic sequences of variable length. Among the proposed marker domains are APS-Reductase (PF12139:  $H' = 1.2$ ), ATP-sulfurilase (PF01747:  $H' = 1.03$ ), and DsrC (PF04358:  $H' = 0.52$ ), key protein families in metabolic pathways involved in both sulfur oxidation/reduction processes. Finally, cluster 2 includes Pfam domains displaying high entropy values and high std, such as the PUA-like domain (PF14306:  $H' = 1$ ). We presume that domains within this cluster are also key players in S-metabolism; however, their high std makes them unsuitable for markers, particularly with metagenomic sequences of variable MSL. We suggest that further analyses will be required to test the implication in S-energy conservation processes of

proteins containing domains such as PF03916, PF02665, or PF14697 (see the complete list in Table S4).

### Is the entropy affected by the input list of microorganisms? Negative control test

In order to evaluate to what extent the  $H'$  values depend on the curated list of microorganisms, we performed a negative control by replacing Suli in 1000 lists of randomly sampled genomes, and we used them to compute the observed frequencies (see Equation (1)). As expected, there was a clear difference between both  $H'$  estimates (see Fig. S5). In particular, entropy values derived from the random test were found to be approximately symmetric and consistently low among the GenF size categories (compared with the real values), yielding values of  $-0.09$  and  $0.1$  as 5th and 95th percentiles, respectively (Table S5).

### Sulfur Score and its predictive capacity to detect S-microbial players in a large genomic dataset

To test whether Pfam entropies can be combined to capture the S-metabolic machinery in "omic" samples, we calculated the final MEBS score, called, in this case, Sulfur Score. We computed the SS on each of the 2107 non-redundant genomes in Gen with the script `score_genomes.sh`. The individual genomes, along with their corresponding SS values and taxonomy according to NCBI, are found in Table S6.



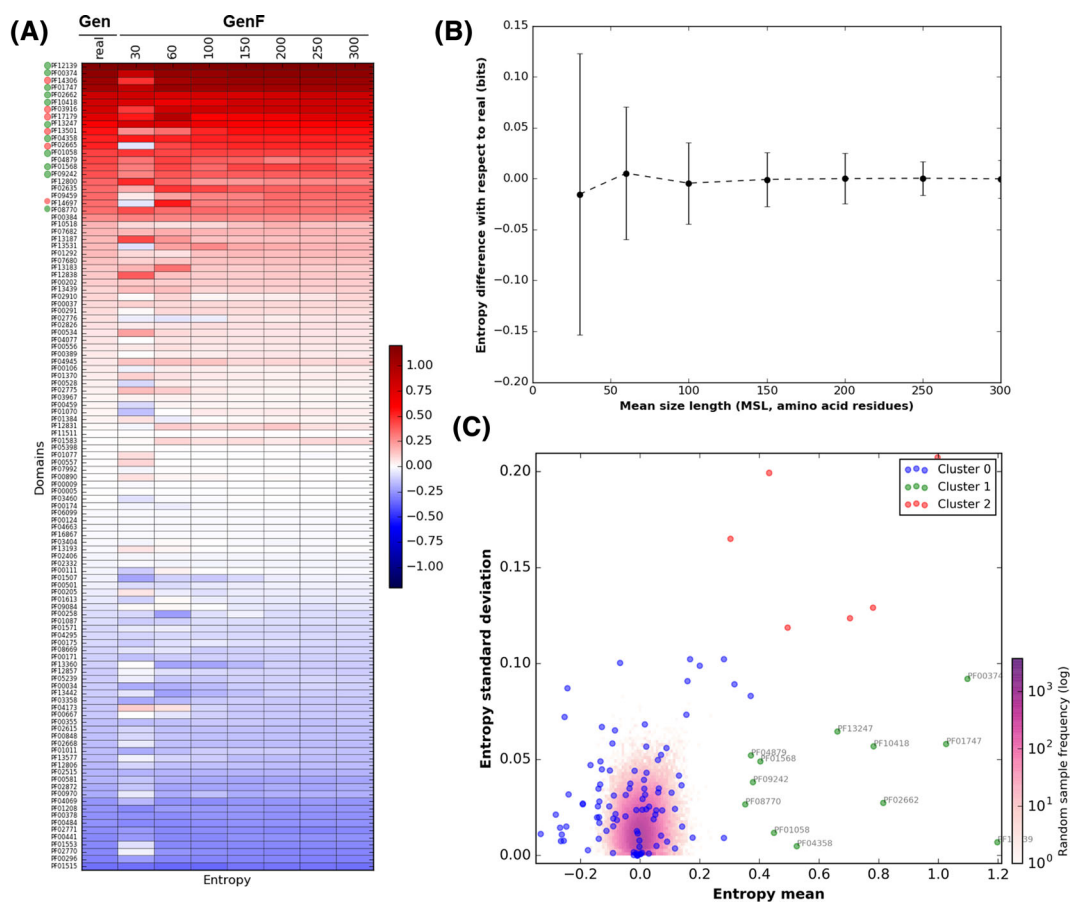


**Figure 4:** Entropy values of Sulfur-derived protein domains. **(A)** Heatmap showing the entropy values ( $H'$ ) of the 112 Pfam domains identified in proteins curated in SuCy. **(B)** Difference between entropies estimated from sizes categories of growing peptide size (GenF) and the real values measured within complete genomes (Gen). Error bars show standard deviations. Both graphs were obtained with script `plot_entropy.py`. Clustering of the Pfam relative entropies obtained in Gen and GenF was produced with the Ward method. Log frequency of the entropy values computed in the random test is colored in purple (see scale bar). Cluster 0 (blue) groups protein domains with low relative entropy that overlap with the random distribution. Cluster 1 (green) includes the Pfam domains that fulfill the requirements to be used as molecular markers (high  $H'$  and low standard deviation [std]). Red dots (cluster 2) correspond to Pfam domains with high  $H'$  and std. The cluster was produced with script `F_meanVStd.py`.

For evaluation purposes, we classified and manually annotated all the genomes in Gen according to their metabolic capabilities. First, we identified the 161 curated genomes belonging to Suli. Then, we focused on the remaining genomes. A set of 192 genomes with  $SS > 4$  were labeled Sulfur unconsidered or related microorganisms (Sur). Finally, the rest of genomes in Gen were classified as NS (Non-Sulfur = Gen - (Suli + Sur)), including 1754 genomes. The boxplots in Fig. 5A summarize the scores obtained in these 3 subsets.

To double-check whether the Sur genomes—selected due to their SS—might be involved in the S-cycle, we manually annotated all of them, focusing on relevant genomic, biochemical, physiological, and environmental information that we might have missed since Suli was first curated (Table S7). Out of 192 genomes, 68 are reported to metabolize S-compounds under culture conditions in the literature. For instance, *Sideroxydans lithotrophicus* ES-1, a microaerophilic Fe-oxidizing bacterium, has been observed to also grow in thiosulfate as an energy source [56]. Another 59 Sur organisms have been isolated from Sulfur-rich environments, such as hot springs or solfataric muds. Remarkably, some of this species include hard-to culture genomes reconstructed from metagenomic sequences such as *Candidatus Desulforudis audaxviator* MP104C isolated from basalt-hosted fluids of the deep subsea floor [6], an unnamed endosymbiont

of a scaly snail from a black smoker chimney [57], and archaeon *Geoglobus ahangari*, sampled from a 2000-meter-deep hydrothermal vent [58]. Furthermore, we also confirmed within Sur the implication of S-cycle of 20 species of the genus *Campylobacter*. These results are consistent with the ecological role of the involved taxa, that along with SRB and methanogens inhabiting host-gastrointestinal and low-oxygen environments, where several inorganic (e.g., sulfates, sulfites) or organic (e.g., dietary amino acids and host mucins) are highly metabolized by these metabolic guilds [59]. The implication of *Campylobacter* species in the S-cycle is also supported by the fact that some of them have been isolated from deep sea hydrothermal vents [60]. The remaining species in Sur were classified into different categories, including bioremediation (7), Fe-environment (2), marine (2), peat lands (2) and other environments (32) (see Fig. 5B).

When the SS values of genomes in Sur are compared to the S-metabolic guilds represented in Suli (e.g., PSB, SRB, GSB), it can be seen that they are indeed similar and clearly separated from the rest of the NS genomes (Fig. 5C). This strongly suggests that high-scoring genomes are indeed ecologically and metabolically implicated in the S-cycle.

Finally, in order to quantify the capacity of the SS to accurately classify S-related microorganisms, we computed a ROC

**Table 2:** Informative Pfam domains with high  $H'$  and low std; novel proposed molecular marker domains in metagenomic data of variable MSL

Pfam ID (Suli occurrences)	$H'$ mean	$H'$ std	Description
PF12139 58/161	1.2	0.01	Adenosine-5'-phosphosulfate reductase beta subunit: key protein domain for both sulfur oxidation/reduction metabolic pathways. Has been widely studied in the dissimilatory sulfate reduction metabolism. In all recognized sulfate-reducing prokaryotes, the dissimilatory process is mediated by 3 key enzymes: Sat, Apr, and Dsr. Homologous proteins are also present in the anoxygenic photolithotrophic and chemolithotrophic sulfur-oxidizing bacteria (CLSB, PSB, GSB), in different cluster organizations [35].
PF00374 135/161	1.1	0.09	Nickel-dependent hydrogenase: hydrogenases with S-cluster and selenium containing Cys-x-x-Cys motifs involved in the binding of nickel. Among the homologues of this hydrogenase domain is the alpha subunit of the sulfhydrogenase I complex of <i>Pyrococcus furiosus</i> that catalyzes the reduction of polysulfide to hydrogen sulfide with NADPH as the electron donor [69].
PF01747 103/161	1.03	0.06	ATP-sulfurylase: key protein domain for both sulfur oxidation and reduction processes. The enzyme catalyzes the transfer of the adenylyl group from ATP to inorganic sulfate, producing adenosine 5'-phosphosulfate (APS) and pyrophosphate, or the reverse reaction [70].
PF02662 62/161	0.82	0.03	Methyl-viologen-reducing hydrogenase, delta subunit: is 1 of the enzymes involved in methanogenesis and encoded in the mth-flp-mvh-mrt cluster of methane genes in <i>Methanothermobacter thermautotrophicus</i> . No specific functions have been assigned to the delta subunit [49].
PF10418 122/161	0.78	0.06	Iron-sulfur cluster binding domain of dihydroorotate dehydrogenase B: among the homologous genes in this family are <i>asrA</i> and <i>asrB</i> from <i>Salmonella enterica enterica serovar Typhimurium</i> , which encode (1) a dissimilatory sulfite reductase, (2) a gamma subunit of the sulfhydrogenase I complex of <i>Pyrococcus furiosus</i> , and (3) a gamma subunit of the sulfhydrogenase II complex of the same organism [12].
PF13247 149/161	0.66	0.06	4Fe-4S dicluster domain: Homologues of this family include: (1) DsrO, a ferredoxin-like protein, related to the electron transfer subunits of respiratory enzymes, (2) dimethylsulfide dehydrogenase $\beta$ subunit ( <i>ddhB</i> ), involved in dimethyl sulfide degradation in <i>Rhodovulum sulfidophilum</i> , and (3) sulfur reductase FeS subunit ( <i>sreB</i> ) of <i>Acidianus ambivalens</i> , involved in sulfur reduction using $H_2$ or organic substrates as electron donors [12].
PF04358 73/161	0.52	0	DsrC like protein: DsrC is present in all organisms encoding a dsrAB sulfite reductase (sulfate/sulfite reducers or sulfur oxidizers). The physiological studies suggest that sulfate reduction rates are determined by cellular levels of this protein. The dissimilatory sulfate reduction couples the 4-electron reduction of the DsrC trisulfide to energy conservation [71]. DsrC was initially described as a subunit of DsrAB, forming a tight complex; however, it is not a subunit, but rather a protein with which DsrAB interacts. DsrC is involved in sulfur-transfer reactions; there is a disulfide bond between the 2 DsrC cysteines as a redox-active center in the sulfite reduction pathway. Moreover, DsrC is among the most highly expressed sulfur energy metabolism genes in isolated organisms and meta-transcriptomes [71].
PF01058 158/161	0.45	0.01	NADH ubiquinone oxidoreductase, 20 Kd subunit: homologous genes are found in the delta subunits of both sulfhydrogenase complexes of <i>Pyrococcus furiosus</i> [12].
PF01568 156/161	0.4	0.05	Molybdopterin dinucleotide binding domain: this domain corresponds to the C-terminal domain IV in dimethyl sulfoxide (DMSO) reductase [49].
PF09242 39/161	0.38	0.04	Flavocytochrome c sulphide dehydrogenase, flavin-binding: enzymes found in S-oxidizing bacteria such as the purple phototrophic bacteria <i>Chromatium vinosum</i> [49].
PF04879 151/161	0.37	0.05	Molybdopterin oxidoreductase Fe4S4 domain: is found in a number of reductase/dehydrogenase families, which include the periplasmic nitrate reductase precursor and the formate dehydrogenase alpha chain, i.e., <i>Wolinella succinogenes</i> polysulfide reductase chain, <i>Salmonella typhimurium</i> thiosulfate reductase (gene <i>phsA</i> ).
PF08770 45/161	0.35	0.03	Sulphur oxidation protein SoxZ: SoxZ sulfur compound chelating protein, part of the complex known as the Sox enzyme system (for sulfur oxidation) that is able to oxidize thiosulfate to sulfate with no intermediates in <i>Paracoccus parantropus</i> [12].

curve (for a detailed description of ROC curves, see [61]). We thus defined genomes annotated in Suli as positive instances, and the rest as negative ones. The results are shown in Fig. 5D, with an estimated area under the curve (AUC) of 0.985, and the corresponding cut-off values of SS for several false positive rates (FPR). According to this test, an SS value of 8.705 is required to

rule out all false positives in Gen, while  $SS = 5.231$  is sufficient to achieve an FPR < 0.05.

Overall, these results indicate that MEBS is a powerful and broadly applicable approach to predict and classify microorganisms closely involved in the sulfur cycle, even in hard-to-culture microbial lineages.

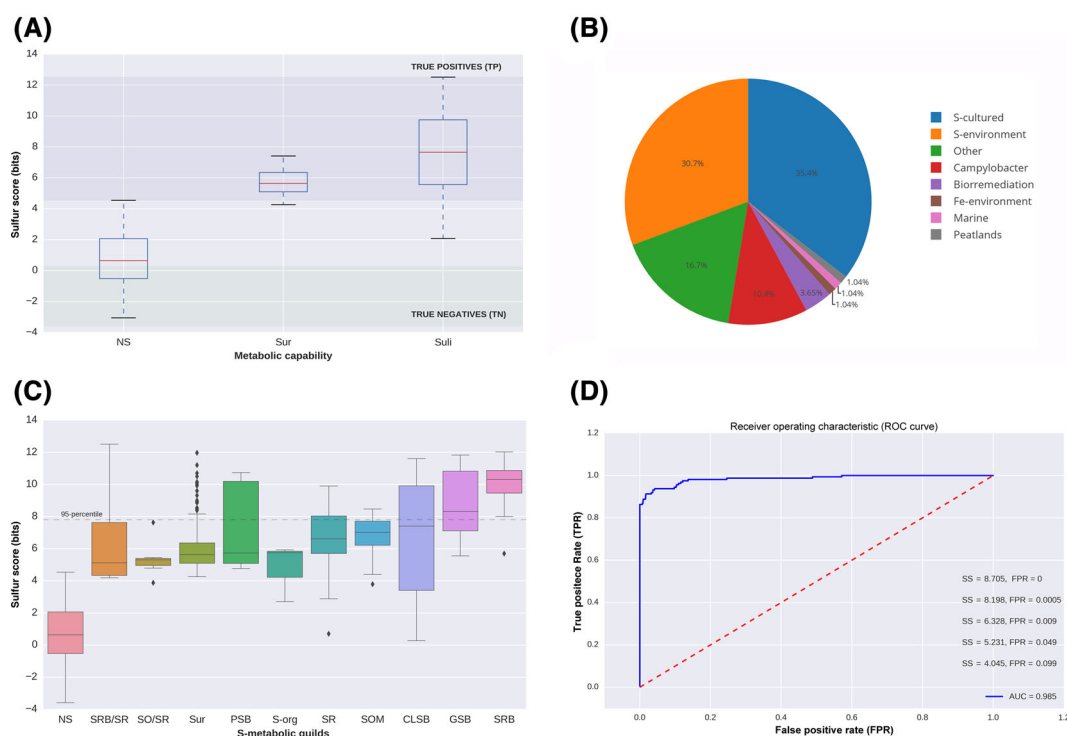


**Figure 5:** Distribution of Sulfur Score (SS) in 2107 non-redundant genomes (Gen). (A) Subsets of genomes annotated in Suli ( $n = 161$ ). (ii) Sur, genomes not listed in Suli with  $SS > 4$  and candidates to be S-related microorganisms ( $n = 192$ ). (iii) Rest of the genomes in Gen (NS,  $n = 1754$ ). According to the curated species, true positives can be defined as genomes with  $SS > \max(SS_{NS})$  distribution, whereas true negatives are those with  $SS < \min(SS_{Suli})$ . (B) Assignment of the 192 genomes in Sur to ecological categories based on literature reports. (C) Distribution of SS for different S-metabolic guilds, and the genomes in Sur. (D) ROC curve with area under the curve (AUC) indicated together, with thresholds for some false positive rates (FPR).

### Sulfur Score and its predictive capacity to detect S-related environments in a large metagenomic collection

The SS was also computed for each metagenome in Met, using their corresponding MSL to choose the appropriate entropies previously calculated in dataset GenF (Table S8). In order to test whether SS values can be used to identify S-related environments, we performed the following analyses. First, we used the geographical metadata associated with each metagenome to map the global distribution of SS. In Fig. 6A, SS values are colored from yellow to red. The most informative S-environments (displaying SS values equal to or greater than the 95th percentile of each MSL category) are shown in blue.

Then, we sorted the metagenomes according to their environmental features, as proposed by the Genomic Standards Consortium (GSC) and implemented in MG-RAST. Each feature corresponds to 1 of 13 environmental packages (EPs) that standardize metadata describing particular habitats that are applicable across all GSC checklists and beyond [62]. Therefore, each EP represents a broad and general classification containing particular features. For example, the “water” EP includes 330 metagenomes from our dataset, belonging to several features such as freshwater, lakes, estuarine, marine, hydrothermal vents, etc. As each of these features has different ecological capabilities in terms of biogeochemical cycles, we can expect different behaviors among SS values, as shown in Fig. 6B. In general, all the metagenomes derived from hydrothermal vents (2), marine benthic (6), intertidal (8), and our unpublished CCC microbial mats had SS values above the 95th percentile, highlighting the importance of the S-cycle in these envi-

ronments. In contrast, the metagenomes belonging to features such as sub-terrestrial habitat (7), saline evaporation pond (24), or organisms-associated habitat (7) displayed consistently low or even negative SS values, indicating a negligible presence of S-metabolic pathways in those environments. The remaining features have intermediate median SS values and contain occasionally individual metagenomes with SS values above the 95th percentile, such as freshwater, marine, ocean, or biofilm environments.

To validate the list of 50 high-scoring metagenomes (above the 95th percentile), we double-checked their annotations. According to the literature and associated metadata, all these environments are closely involved in the mineralization, uptake, and recycling processes of S-compounds, e.g., environmental sequences derived from the coastal Oligochaete worm *Olavius algarvensis*, hydrothermal vents, and marine deep-sea surface sediments around the Deep-Water Horizon spill in the Gulf of Mexico. The complete list of annotated metagenomes, along with their ecological capabilities, is found in Table S9.

### Evaluating the robustness of the sulfur score

To test the reproducibility and robustness of the MEBS final score (SS), we conducted 2 further analyses. In the first, we compared SS estimates derived from the Met dataset, computed with Pfam entropies obtained in the first MEBS benchmark performed 3 years ago (2014) with the current data described in this article (2017). Despite the changes of both databases (Pfam database version and the Suli list), we found a strong correlation ( $r^2 = 0.912$ ) between the SS outcomes (Fig. S6 A). A kernel density analysis of the latter comparison suggests a different behavior of low

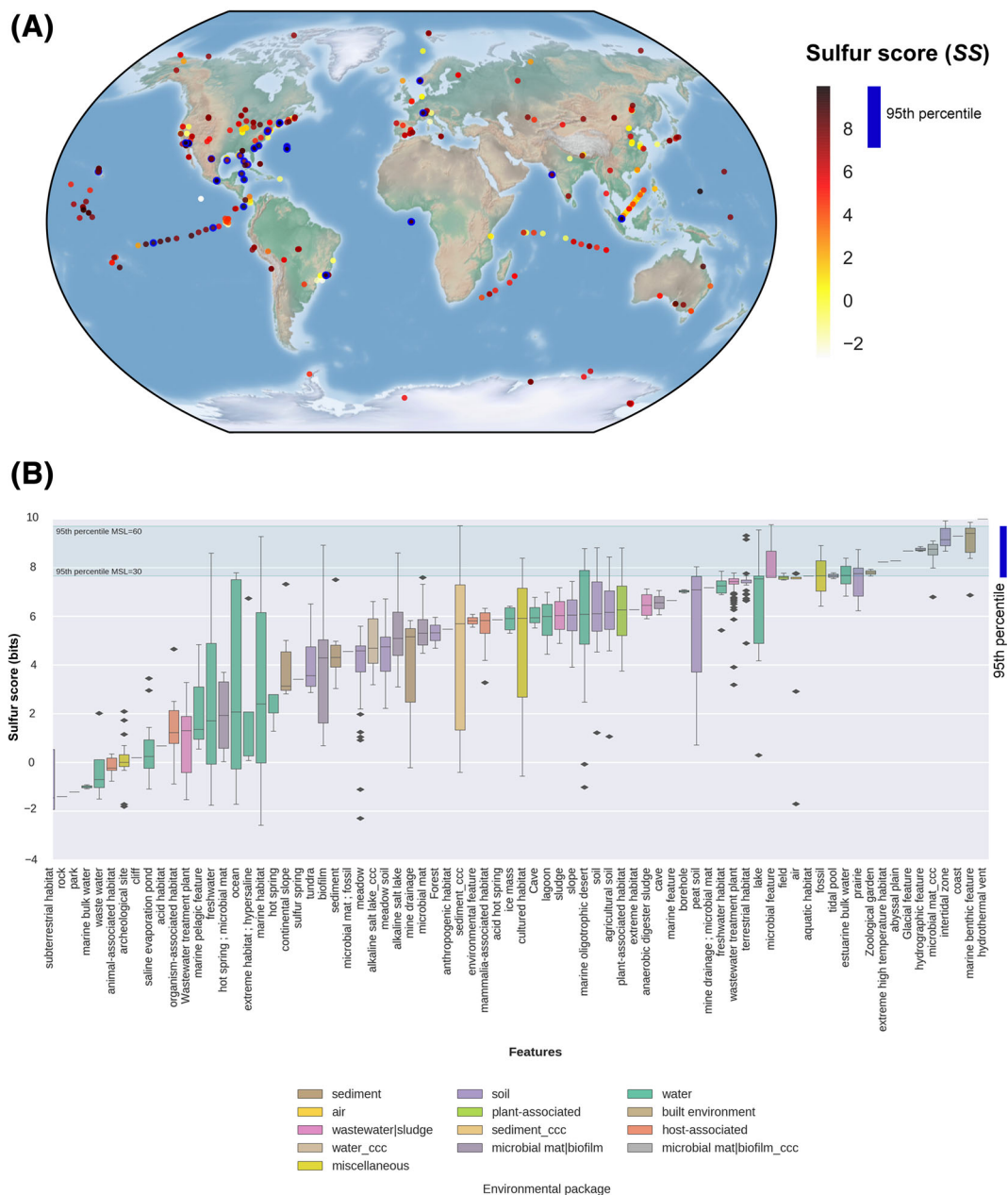


**Figure 6:** Distribution of Sulfur Score (SS) in the metagenomic dataset Met. **(A)** Geo-localized metagenomes sampled around the globe are colored according to their SS values. The following cut-off values correspond to the 95th percentiles of 7 mean size length classes (30, 60, 100, 150, 200, 250, and 300 aa): 7.66, 9.70, 8.81, 8.51, 8.18, 8.98, and 7.61, respectively. Circles with a thick blue border indicate metagenomes with  $SS \geq$  the 95th percentile. **(B)** Distribution of SS values observed in 935 metagenomes classified in terms of features (x-axis) and colored according to their particular habitats. Features are sorted according to their median SS values. ccc: metagenomes from Cuatro Ciénegas, Coahuila, Mexico. Green lines indicate the lowest and largest 95th percentiles observed across MSL classes.

and high SS scores, with the latter being more reproducible (see Fig. S6B).

In the second analysis, we quantitatively tested to what extent the entropy estimates of the 112 Pfam domains directly affect the outcome of the SS in Gen and Met. We randomly subsampled  $\approx 50\%$  of those domains to compute the SS a thousand times for each genome and metagenome in Gen and Met, respectively. The results, summarized in Table S10, confirm that SS values computed with random subsets of Pfam domains are generally lower than SS derived from the full list ( $n = 112$ ) of SUCY-Pfam domains. To further inspect the distribution of SS values produced with random subsets of domains (random SS), we

focused on the particular case of the metagenomes belonging to the category  $MSL = 60$ . As expected, the distribution of random SS oscillates between negative and positive values. Interestingly, metagenomes exhibiting only positive random SS are ranked above the 95th percentile according to their real SS values (see Fig. S7A). The latter indicates that even a random subset of Pfam domains used to compute the score is more likely to highly rank metagenomes containing the sulfur metabolic machinery (large number of high-entropy Pfam domains), than those lacking the sulfur metabolism or displaying a large number of non-informative Pfam domains. Furthermore, by comparing the median of random SS with the real scores, we observe

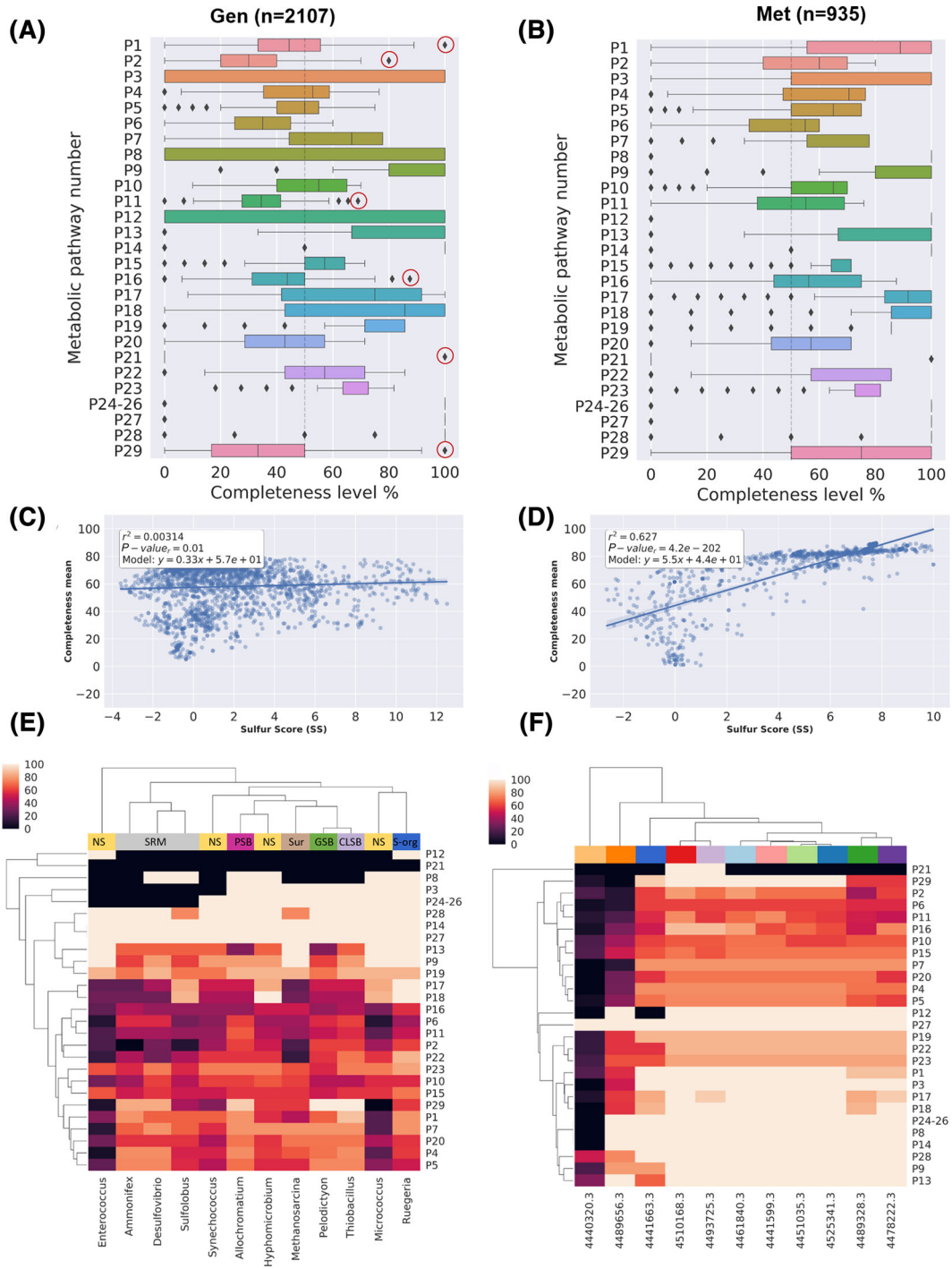


**Figure 7:** Metabolic completeness of the metabolic pathways described in Table 1. **(A)** Boxplot distribution of the pathway completeness in genomic and **(B)** metagenomic datasets. **(C)** Linear regression models of the Sulfur Score (SS) and the mean completeness in Gen and **(D)** Met dataset. **(E)** Heatmap showing the metabolic completeness of the following genomes: *Desulfovibrio vulgaris* DP4 (SS = 11.442), *Ammonifex degensii* KC4 (SS = 12.508); *Pelodictyon phaeoclathratiforme* BU-1 (SS = 11.836); *Thiobacillus denitrificans* ATCC 25 259 (SS = 11.61); PSB: *Allochromatium vinosum* DSM 180 (SS = 10.737); SUR: *Sur Methanosarcina barkeri* MS (SS = 5.93); *Sulfolobus acidocaldarius* DSM 639 (SS = 5.457); *Synechococcus* sp. JA-2-3Ba 2-13 (SS = 3.704); *Hyphomicrobium denitrificans* 1NES1 (SS = 3.236); *Ruegeria pomeroyi* DSS-3 (SS = 2.707); *Enterococcus durans* (SS = -0.194); *Micrococcus luteus* NCTC.2665 (SS = -3.588). **(F)** Heatmap showing the metabolic completeness of the metagenomes with the following MG-RAST IDs and corresponding scores: 4489656.3 (SS = -2.649); 4440320.3 (SS = 0.1); 4441663.3 (SS = 9.986); 4510168.3 (SS = 7.781); 4493725.3 (SS = 9.547); 4461840.3 (SS = 8.813); 4441599.3 (SS = 9.274); 4451035.3 (SS = 9.918); 4525341.3 (SS = 9.287); 4489328.3 (SS = 4.958); 4478222.3 (SS = 4.88). The color codes at the top of the heatmap correspond to different environments. For a more detailed description of each metagenome, see Table S8.

a clear separation between those distributions (see Fig. S7B and Table S10).

### Completeness of S-metabolic pathways

As we described above, the MEBS pipeline models a metabolic network as an array of S-related protein domains (Sucy-Pfam) to ultimately use their entropies to produce the final score (SS). For a closer look, we also dissected the total contribution of independent domains at the network level in order to assess whether SS depends on the partial or complete detection of S-pathways. Consequently, we evaluated the pathway completeness in both genomic (Gen) and metagenomic (Met) datasets (see Tables S11 and S12, respectively). Since the number of Pfam domains per pathway goes from 1 to 29 (see Table 1 and Table S2), we suspect that pathways represented by a single domain might not reflect their complete metabolic function. For example, the pathways involved in the methanogenesis of compounds such as dimethylsulfide (DMS, P24), methyl-thiolpropanoate (MTPA, P25), and methanethiol (MeSH, P26) are represented by the same protein (MtsA, PF01208) in our Sucy database, as well as in Metacyc [12]. Therefore, we expect that pathways P24–26 will have identical presence-absence patterns in Gen and Met.

The boxplots in Fig. 7A and B summarize the distribution of completeness for each S-metabolic pathway, including the synthetic pathway (P29) composed by 12 candidate markers as described in Table 2. As expected, the observed completeness per pathway was higher in Met than in Gen, since microbial communities harbor a wider repertory of metabolic functions than single genomes. In the case of genomes, we noted that a few pathways were complete in most genomes, the majority being involved in the usage of organic sulfur compounds such as alkanesulfonates (P9), sulfoacetate (P14), and biosynthesis of sulfolipids (SQDG) and the single domain pathways P24–26. Remarkably, we also detected a few organisms displaying the highest levels of metabolic completeness in some S-energy based pathways. For example, we found that *Desulfosporosinus acidiphilus* SJ4 (SS = 8.91) was the only genome harboring the complete repertory of Pfam domains described in Sucy for the sulfite oxidation (P1), strongly suggesting that it may oxidize sulfite. However, this activity remains to be tested in culture [63]. In the case of thiosulfate oxidation (P3), we detected 3 genomes displaying the highest levels of completeness, in agreement with their ecological features: *Hydrogenobaculum* sp. Y04AAS1 (SS = 9.319) [64] and the CLSB: *Acidithiobacillus caldus* ATCC 51756 (SS = 6.525) [65] and *Acidithiobacillus ferrivorans* (SS = 7.436) [66]. For the sulfate reduction dissimilative pathway (P5), out of 55 genomes displaying the higher completeness levels, 67% are actually SRB, 12% are Sur genomes, and the rest are sulfur oxidation microorganisms. Furthermore, the PSB *Thioflaviccoccus mobilis* 8321 (SS = 9.756), isolated from a microbial mat [67], was the genome displaying the most complete sulfide oxidation pathway (P11). Elemental sulfur disproportionation (P21) is represented by a single non-informative domain (PF07682,  $H' = 0.172$ ) that remarkably is found in 14 sulfur respiring or related genomes such as *Sulfolobus tokodaii* str. 7 (SS = 5.341) and *Acidianus hospitalis* W1 (SS = 3.88). Finally, we identified 6 genomes encoding all 12 proposed markers. Among them, 3 were GSB (*Pelodictyon phaeoclathratiforme* BU-1, SS = 11.836, *Chlorobium chlorochromatii* CaD3, SS = 11.625, and *Chlorobium tepidum* TLS, SS = 11.354), 1 CLSB (*Thiobacillus denitrificans* ATCC 25259 SS = 11.61), another 1 PSB (*Thiocystis violascens* DSM 198, SS = 10.633), and finally 1 Sur (*Sedimenticola thiotaurini* SS = 10.109). For a complete description, see Table S13.

A global view of metabolic completeness was obtained by bulking the data from all pathways. Linear regression models between mean completeness and SS that were computed confirm the yielding  $r^2$  values of 0.003 and 0.627 for Gen and Met, respectively (See Fig. 7C and D). Moreover, we also assessed the relationship between the mean completeness of the synthetic pathway of candidate markers (P29) and the SS. As expected, significant correlations were obtained in both datasets ( $r^2 = 0.645$  and  $r^2 = 0.881$  for Gen and Met, respectively) (see Fig. S8).

To get a more detailed insight into the completeness, we selected a few genomes and metagenomes displaying high and low SS values. Specifically, from the Gen dataset, we selected 1 representative from the main S-guilds, 1 Sur genome, and 2 genomes with low SS values (NS). As observed in Fig. 7, the low-scoring genomes *Enterococcus durans* (SS = -0.194), *Micrococcus luteus* NCTC\_2665 (SS = -3.588), and *Ruegeria pomeroyi* DSS-3 (SS = 2.707) display unrelated patterns of sulfur metabolic completeness compared with the rest of the genomes and therefore are separated. In contrast, high-scoring S-respiring microorganisms *Desulfovibrio vulgaris* DP4 (SS = 11.442), *Sulfolobus acidocaldarius* DSM 639 (SS = 5.457), and *Ammonifex degensii* KC4 (SS = 12.508) are clustered together. We also observed that mat-isolated cyanobacteria *Synechococcus* sp. JA-2-3Ba 2-13, classified as NS with SS = 3.704, was clustered together with other high-scoring genomes, in agreement with the lack of correlation reported above.

In the case of metagenomes (see Fig. 7E), we observed a clear correlation between SS and completeness. For example, metagenomes 4440320.3 and 4489656.3, with the lowest scores (SS = 0.1 and SS = -2.649, respectively), also exhibit the largest number of incomplete pathways. Similarly, high-scoring metagenomes derived from black smoker or marine sediment are grouped together in terms of completeness.

### Conclusions

Our study represents the first exploration of the Sulfur biogeochemical cycle in a large collection of genomes and metagenomes. The manually curated effort resulted in an inventory of the compounds, genes, proteins, molecular pathways, and microorganisms involved. This complex universe of articulated data was reduced to a list of microorganisms and Pfam domains encoded in the proteins that take part in that network. These domains were first ranked in terms of relative entropy, and then summed to produce a single S-score representing the relevance of a given genomic or metagenomic sample in terms of sulfur metabolic machinery. We took advantage of the mathematical framework of information theory, which has been widely used in computational biology.

The performance of the MEBS pipeline (designed for the above-mentioned tasks) was benchmarked on large genomic and metagenomic sets. Our results support the broad applicability of this algorithm in order to classify annotated genomes as well as newly sequenced environmental samples without prior culture. We also assessed to what extent the final score depended on the partial or complete detection of pathways and observed a higher completeness per pathway in metagenomic sequences than in individual genomes.

We demonstrated that a measurable score can be applied to evaluate any given metabolic machinery or biogeochemical cycle in large (meta)genomic scale, holding the potential to dramatically change the current view of inferring metabolic capabilities in the present “omic” era.

## Availability and requirements

Project name: MEBS

Project home page: [https://github.com/eead-csic-compbio/metagenome\\_Pfam\\_score](https://github.com/eead-csic-compbio/metagenome_Pfam_score)

Operating system(s): Linux

Programming language: Python 3, Perl5, Bash,

Other requirements: HMMER

License: GNU General Public License (GPL)

## Availability of supporting data

The datasets supporting the results of this article and snapshots of the MEBS code in GitHub are available in the *GigaDB* repository [68].

## Supplementary files

The supplementary pdf file contains the following information:

Supplementary figure S1: Histogram distribution of the mean size length of metagenomes in Met and the input sulfur proteins.

Supplementary figure S2: Visualization of the Pfam domains mapped onto KEGG metabolic pathways.

Supplementary figure S3: Comparison of clustering methods of the 112 Pfam entropies using script `plot_cluster_comparison.py`.

Supplementary figure S4: Clustering comparison between Birch and Ward clustering methods to stand out the Pfam entropies with high  $H'$  and low std using the script.

Supplementary figure S5: Distribution of entropy values of 112 Pfam domains inferred from random-sampled and Suli genomes.

Supplementary figure S6: Comparison of Sulfur Scores (SS) with data obtained 3 years ago (2014), with the current data described in the article.

Supplementary table S4: Informative Pfam's with high  $H'$  and high std (not used as molecular marker genes) in metagenomic fragmented data.

Supplementary table S5: Percentile distribution of the 112 Pfam entropies in the random test.

Supplementary table S10: Statistics of SS computed on genomic (Gen, real sequences) and metagenomic (Met, with increasing mean size length, from 30 to 300 aa) datasets.

In separated Excel files, the following supplementary tables are also provided:

Supplementary table S1: Table S1. Comprehensive list of the taxonomic representatives of sulfur cycle including Sulfur list, or "Suli," containing 161 curated genomes used as input for the pipeline.

Supplementary table S2: Suci database containing the identifiers of the Sulfur proteins and their corresponding annotations derived from Interproscan and manual curation.

Supplementary table S3: Sulfur Pfam domains (Pfam-Suci), and their corresponding mapping into KEGG (KO number), and the manual assignment into sulfur metabolic pathways.

Supplementary table S6: Gen dataset containing their corresponding SS and taxonomy assignment.

Supplementary table S7: Manual annotation of Sulfur unconsidered or related microorganisms (Sur) with Sulfur Score (SS) greater or equal to four.

Supplementary table S8: Met dataset with corresponding SS values and metadata.

Supplementary table S9: Manually annotated high-scoring metagenomes along with their ecological capabilities in terms of sulfur cycle.

Supplementary table S11: Metabolic completeness in Gen dataset for each of the 28 metabolic pathways of the S-cycle described in Table 1. (Pathway 29 contains the proposed marker genes.)

Supplementary table S12: Metabolic completeness in Men dataset for each of the 28 metabolic pathways of the S-cycle described in Table 1. (Pathway 29 contains the proposed marker genes.)

Supplementary table S13: Frequency and description of the most complete genomes in terms of S-cycle metabolic pathways.

## Abbreviations

AUC: area under the curve; CCC: Cuatro Ciénegas, Coahuila; CLSB: color-less sulfur bacteria; EP: environmental packages; ESR: elemental sulfur-reducing microorganisms; FPR: false positive rate; Gen: genomic dataset; GenF: genomic fragmented dataset; GSB: green sulfur bacteria; GSC: Genomic Standards Consortium; HMM: Hidden Markov Models; MEBS: Multigenomic Entropy Based Score; Met: metagenomic dataset; MSL: mean size length,  $H'$ : relative entropy; NS: non-sulfur-related genomes; PSB: purple sulfur bacteria; Rlist: random list of taxonomic representatives; ROC: receiver operating characteristic; S: sulfur; S-cycle: sulfur cycle; SOM: sulfur-oxidizing microorganisms; SRB: sulfate-reducing bacteria; SS: Sulfur Score; Suci: Sulfur Cycle Database; Suli: Sulfur list; Sur: Sulfur unconsidered; TPR: true positive rate.

## Funding

Valerie De Anda is a doctoral student from Programa de Doctorado en Ciencias Biomédicas, Universidad Nacional Autónoma de México (UNAM), and received fellowship 356 832 from Consejo Nacional de Ciencia y Tecnología (CONACYT). This research was also supported by funding from World Wildlife Fund (WWF)-Alianza Carlos Slim, Sep-Ciencia Básica Conacyt grant 238 245 to both Valeria Souza and Luis Enrique Eguiarte and Spanish MINECO grant CSIC13-4E-2490. Bruno Contreras Moreira was funded by Fundación ARAID. The sabbatical leaves of Luis Enrique Eguiarte and Valeria Souza at the University of Minnesota were supported by scholarships from Programa de Apoyos para la Superación del Personal Académico de la UNAM (PASPA), Dirección General de Asuntos del Personal Académico (DGAPA), UNAM.

## Competing interest

The authors declare that they have no competing interests.

## Author contribution

V.D.A., B.C.M., and I.Z.P. wrote the paper. B.C.M., V.D.A., and A.C.P.H. developed and wrote the software and performed all the bioinformatics analyses. V.D.A. produced all the figures and wrote the documentation of the software. V.D.A. and I.Z.P. conceived the manual curation of the Sulfur Cycle Inventory and the microbiological, biogeochemical, and ecological interpretation. L.E. and V.S. provided the intellectual framework, expertise, and resources to develop and supervise the project. All the authors read and approved the final manuscript.

## Endnotes

We are currently finishing the analyses to demonstrate the applicability of this approach to other biogeochemical cycles (C, N, O, Fe, P). Thereby, we hope that the pipeline MEBS will facilitate analysis of biogeochemical cycles or complex metabolic networks carried out by specific prokaryotic guilds, such as bioremediation processes (i.e., degradation of hydrocarbons, toxic aromatic compounds, heavy metals, etc.). We look forward to collaborating with and helping other researchers by integrating comprehensive databases that might be helpful to the scientific community. Furthermore, we are currently working to improve the algorithm by using only a list of sequenced genomes involved in the metabolism of interest in order to reduce the manual curation effort. We are also considering taking *k-mers* instead of peptide Hidden Markov Models to increase the speed of the pipeline. We anticipate that our platform will stimulate interest and involvement among the scientific community to explore uncultured genomes derived from large metagenomic sequences.

## Acknowledgments

The authors gratefully acknowledge Emilio Morella for his valuable support, feedback, and comments throughout the development of this project. We really appreciate the reviewers Daan Speth and Thulani Makhalanyane, whose valuable comments and suggestions improved the manuscript and software. Our special thanks to Carlos P. Cantalapiedra, Seth Barribeau, Will Levitt, and anonymous reviewers for their comments on earlier versions of the manuscript; these comments immensely improved the algorithm and the final version of the article. The authors also thank the Laboratory of Computational and Structural Biology (EEAD-CSIC) and Laboratorio de Evolución Molecular y Experimental, Instituto de Ecología, UNAM, for providing the computational resources described in the article. The paper was written during a sabbatical leave of Luis Enrique Eguiarte and Valeria Souza (VS) at the University of Minnesota in Peter Tiffin's and Michael Travisano's laboratories.

## References

1. Thomas T, Gilbert J, Meyer F. Metagenomics - a guide from sampling to data analysis. *Microb Inform Exp* 2012;**2**(1):3.
2. Oulas A, Pavloudi C, Polymenakou P et al. Metagenomics: tools and insights for analyzing next-generation sequencing data derived from biodiversity studies. *Bioinf Biol Insights* 2015;**9**:75–88.
3. Morales SE, Holben WE. Linking bacterial identities and ecosystem processes: can 'omic' analyses be more than the sum of their parts? *FEMS Microbiol Ecol* 2011;**75**(1):2–16.
4. Hug LA, Baker BJ, Anantharaman K et al. A new view of the tree of life. *Nat Microbiol* 2016;**1**(5):16048.
5. Marco D. Metagenomics: Current Innovations and Future Trends. Poole, UK: Caister Academic Press; 2011.
6. Jungbluth SP, Glavina Del Rio T, Tringe SG et al. Genomic comparisons of a bacterial lineage that inhabits both marine and terrestrial deep subsurface systems. *PeerJ* 2017;**5**:e3134.
7. Iverson V, Morris RM, Frazar CD et al. Untangling genomes from metagenomes: revealing an uncultured class of marine euryarchaeota. *Science* 2012;**335**(6068):587–90.
8. Sangwan N, Xia F, Gilbert JA. Recovering complete and draft population genomes from metagenome datasets. *Microbiome* 2016;**4**(1):8.
9. Mehrshad M, Amoozegar MA, Ghai R et al. Genome reconstruction from metagenomic data sets reveals novel microbes in the brackish waters of the Caspian Sea. *Appl Environ Microbiol* 2016;**82**(5):1599–612.
10. Sharon I, Banfield JF. Genomes from metagenomics. *Science* 2013;**342**(6162):1057–8.
11. Hiraoka S, Yang C, Iwasaki W. Metagenomics and bioinformatics in microbial ecology: current status and beyond. *Microbes Environ* 2016;**31**(3):204–12.
12. Caspi R, Altman T, Dreher K et al. The MetaCyc database of metabolic pathways and enzymes and the BioCyc collection of pathway/genome databases. *Nucleic Acids Res* 2012;**40**(D1):D742–53.
13. Kanehisa M. KEGG: Kyoto Encyclopedia of Genes and Genomes. *Nucleic Acids Res* 2000;**28**(1):27–30.
14. Ye Y, Doak TG. A parsimony approach to biological pathway reconstruction/inference for metagenomes. *PLoS Comput Biol* 2011;**5**:453–60.
15. Abubucker S, Segata N, Goll J et al. Metabolic reconstruction for metagenomic data and its application to the human microbiome. *PLoS Comput Biol* 2012;**8**(6):e1002358.
16. Larsen PE, Collart FR, Field D et al. Predicted Relative Metabolomic Turnover (PRMT): determining metabolic turnover from a coastal marine metagenomic dataset. *Microb Inform Exp* 2011;**1**(1):4.
17. Hanson NW, Konwar KM, Hawley AK et al. Metabolic pathways for the whole community. *BMC Genomics* 2014;**15**:619.
18. Castañeda LE, Barbosa O. Metagenomic analysis exploring taxonomic and functional diversity of soil microbial communities in Chilean vineyards and surrounding native forests. *PeerJ* 2017;**5**:e3098.
19. Fierer N, Leff JW, Adams BJ et al. Cross-biome metagenomic analyses of soil microbial communities and their functional attributes. *Proc Natl Acad Sci U S A* 2012;**109**:21390–5.
20. Llorens-Marès T, Yooseph S, Goll J et al. Connecting biodiversity and potential functional role in modern euxinic environments by microbial metagenomics. *ISME J* 2015;1–14.
21. Quaiser A, Zivanovic Y, Moreira D et al. Comparative metagenomics of bathypelagic plankton and bottom sediment from the Sea of Marmara. *ISME J* 2011;**5**:285–304.
22. Xie W, Wang F, Guo L et al. Comparative metagenomics of microbial communities inhabiting deep-sea hydrothermal vent chimneys with contrasting chemistries. *ISME J* 2011;**5**:414–26.
23. Delmont TO, Malandain C, Prestat E et al. Metagenomic mining for microbiologists. *ISME J* 2011;**5**:1837–43.
24. Ganesh S, Parris DJ, Delong EF et al. Metagenomic analysis of size-fractionated picoplankton in a marine oxygen minimum zone. *ISME J* 2014;**8**:187–211.
25. Segata N, Izard J, Waldron L et al. Metagenomic biomarker discovery and explanation. *Genome Biol* 2011;**12**:R60.
26. Parks DH, Tyson GW, Hugenholtz P et al. STAMP: statistical analysis of taxonomic and functional profiles. *Bioinformatics* 2014;**30**:3123–4.
27. Sohn MB, Du R, An L. A robust approach for identifying differentially abundant features in metagenomic samples. *Bioinformatics* 2015;**31**:2269–75.
28. Kullback S, Leibler RA. On information and sufficiency. *Ann Math Stat* 1951;**22**:79–86.
29. Commenges D. Information theory and statistics: an overview. 2015;1–22.
30. Hertz GZ, Stormo GD. Identifying DNA and protein patterns with statistically significant alignments of multiple sequences. *Bioinformatics* 1999;**15**:563–77.



31. Dar SA, Yao L, Van Dongen U et al. Analysis of diversity and activity of sulfate-reducing bacterial communities in sulfidogenic bioreactors using 16S rRNA and *dsrB* genes as molecular markers. *Appl Environ Microbiol* 2007;**73**:594–604.
32. Perez-Jimenez JR, Kerkhof LJ. Phylogeography of sulfate-reducing bacteria among disturbed sediments, disclosed by analysis of the dissimilatory sulfite reductase genes (*dsrAB*). *Appl Environ Microbiol* 2005;**71**:1004–11.
33. Loy A, Duller S, Baranyi C et al. Reverse dissimilatory sulfite reductase as phylogenetic marker for a subgroup of sulfur-oxidizing prokaryotes. *Environ Microbiol* 2009;**11**:289–99.
34. Hügler M, Gärtner A, Imhoff JF. Functional genes as markers for sulfur cycling and CO<sub>2</sub> fixation in microbial communities of hydrothermal vents of the Logatchev field. *FEMS Microbiol Ecol* 2010;**73**:526–37.
35. Meyer B, Kuever J. Molecular analysis of the diversity of sulfate-reducing and sulfur-oxidizing prokaryotes in the environment, using *aprA* as functional marker gene. *Appl Environ Microbiol* 2007;**73**:7664–79.
36. Multigenomic Entropy Based Score pipeline (MEBS). [https://github.com/eead-csic-compbio/metagenome\\_Pfam\\_score](https://github.com/eead-csic-compbio/metagenome_Pfam_score). Accessed 5 October 2017.
37. Enzyme nomenclature. <http://enzyme.expasy.org/>. Accessed 5 May 2016.
38. Magrane M, Consortium U. UniProt Knowledgebase: a hub of integrated protein data. *Database* 2011;**2011**:bar009-.
39. Reference and representative genomes. <https://www.ncbi.nlm.nih.gov/genome/browse/reference/>. Accessed 21 December 2016.
40. Genome clusters. <http://microbiome.wlu.ca/research/redundancy/redundancy.cgi>. Accessed 21 December 2016.
41. Moreno-Hagelsieb G, Wang Z, Walsh S et al. Phylogenomic clustering for selecting non-redundant genomes for comparative genomics. *Bioinformatics* 2013;**29**:947–9.
42. NCBI genome assembly summary file. [ftp://ftp.ncbi.nlm.nih.gov/genomes/refseq/assembly\\_summary\\_refseq.txt](ftp://ftp.ncbi.nlm.nih.gov/genomes/refseq/assembly_summary_refseq.txt). Accessed 21 December 2016.
43. NCBI. NCBI FTP site. <ftp://ftp.ncbi.nlm.nih.gov/genomes/all/>. Accessed 21 December 2016.
44. MG-RAST. <http://metagenomics.anl.gov/>. Accessed 10 November 2016.
45. MG-RAST API. <http://api.metagenomics.anl.gov/api.html>. Accessed 15 November 2016.
46. Prakash T, Taylor TD. Functional assignment of metagenomic data: challenges and applications. *Brief Bioinform* 2012;**13**:711–27.
47. Zhong C, Yang Y, Yooseph S. GRASP: guided reference-based assembly of short peptides. *Nucleic Acids Res* 2015;**43**:e18.
48. Jones P, Binns D, Chang H-Y et al. InterProScan 5: genome-scale protein function classification. *Bioinformatics* 2014;**30**:1236–40.
49. Finn RD, Tate J, Mistry J et al. The Pfam protein families database. *Nucleic Acids Res* 2008;**36**:D281–8.
50. Haft DH. The TIGRFAMs database of protein families. *Nucleic Acids Res* 2003;**31**:371–3.
51. Gough J, Chothia C. SUPERFAMILY: HMMs representing all proteins of known structure. SCOP sequence searches, alignments and genome assignments. *Nucleic Acids Res* 2002;**30**:268–72.
52. Finn RD, Clements J, Eddy SR. HMMER web server: interactive sequence similarity searching. *Nucleic Acids Res* 2011;**39**:W29–37.
53. Pedregosa F, Varoquaux G, Gramfort A et al. Scikit-learn: machine learning in Python. *J Mach Learn Res* 2011;**12**:2825–30.
54. KEGG Mapper. <http://www.genome.jp/kegg/mapper.html>. Accessed 4 September 2017.
55. Alcaraz LD, Olmedo G, Bonilla G et al. The genome of *Bacillus coahuilensis* reveals adaptations essential for survival in the relic of an ancient marine environment. *Proc Natl Acad Sci U S A* 2008;**105**:5803–8.
56. Emerson D, Field EK, Chertkov O et al. Comparative genomics of freshwater Fe-oxidizing bacteria: implications for physiology, ecology, and systematics. *Front Microbiol* 2013;**4**:254.
57. Nakagawa S, Shimamura S, Takaki Y et al. Allying with armored snails: the complete genome of gammaproteobacterial endosymbiont. *ISME J* 2014;**8**:40–51.
58. Manzella MP, Holmes DE, Rocheleau JM et al. The complete genome sequence and emendation of the hyperthermophilic, obligate iron-reducing archaeon “*Geoglobus ahangari*” strain 234T. *Stand Genomic Sci* 2015;**10**:77.
59. Carbonero F, Benefiel AC, Alizadeh-Ghamsari AH et al. Microbial pathways in colonic sulfur metabolism and links with health and disease. *Front Physiol* 2012;**1**:1–11.
60. Nakagawa S, Takaki Y, Shimamura S et al. Deep-sea vent—proteobacterial genomes provide insights into emergence of pathogens. *Proc Natl Acad Sci U S A* 2007;**104**:12146–50.
61. Fawcett T. An introduction to ROC analysis. *Pattern Recognit Lett* 2006;**27**:861–74.
62. Field D, Sterk P, Kottmann R et al. Genomic standards consortium projects. *Stand Genomic Sci* 2014;**9**(3):599–601.
63. Alazard D, Joseph M, Battaglia-Brunet F et al. *Desulfosporosinus acidiphilus* sp. nov.: a moderately acidophilic sulfate-reducing bacterium isolated from acid mining drainage sediments. *Extremophiles* 2010;**14**:305–12.
64. Romano C, D’imperio S, Woyke T et al. Comparative genomic analysis of phylogenetically closely related *Hydrogenobaculum* sp. isolates from Yellowstone National Park. *Appl Environ Microbiol* 2013;**79**:2932–43.
65. Chen L, Ren Y, Lin J et al. *Acidithiobacillus caldus* sulfur oxidation model based on transcriptome analysis between the wild type and sulfur oxygenase reductase defective mutant. *PLoS One* 2012;**7**:e39470.
66. Liljeqvist M, Valdes J, Holmes DS et al. Draft genome of the psychrotolerant acidophile *Acidithiobacillus ferrivorans* SS3. *J Bacteriol* 2011;**193**:4304–5.
67. Imhoff JF, Pfennig N. *Thioflavicoccus mobilis* gen. nov., sp. nov., a novel purple sulfur bacterium with bacteriochlorophyll b. *Int J Syst Evol Microbiol* 2001;**51**:105–10.
68. De Anda V, Zapata-Penasco I, Poot-Hernandez AC et al. Multigenomic Entropy Based Score (MEBS): the molecular reconstruction of the sulfur cycle. *GigaScience Database* 2017. <http://dx.doi.org/10.5524/100357>.
69. Pedroni P, Volpe AD, Galli G et al. Characterization of the locus encoding the [Ni-Fe] sulfhydrylase from the archaeon *Pyrococcus furiosus*: evidence for a relationship to bacterial sulfite reductases. *Microbiology* 1995;**141**:449–58.
70. Taguchi Y, Sugishima M, Fukuyama K. Crystal structure of a novel zinc-binding ATP sulfurylase from *Thermus thermophilus* HB8. *Biochemistry* 2004;**43**(14):4111–8.
71. Santos AA, Venceslau SS, Grein F et al. A protein trisulfide couples dissimilatory sulfate reduction to energy conservation. *Science* 2015;**350**:1541–5.